A Density Functional Study of the Highly Adaptable Molecular Structure of Mo(V) and W(V) Dithiolene Complexes: From Three-Dimensional Antiferromagnet to Spin Ladder

Benoît Domercq,[1a] Claude Coulon,[1b] and Marc Fourmigué*,[1a]

Sciences Moléculaires aux Interfaces, FRE CNRS 2068, Institut des Matériaux Jean Rouxel, BP 32229, 2, rue de la Houssinière, 44322 Nantes Cedex 3, France, and Centre de Recherches Paul Pascal, CNRS, av. Dr. Schweitzer, 33600 Pessac, France

Received May 23, 2000

Cp_2M(dithiolene) (M = Mo^{IV}, W^{IV}) d^2 complexes exhibit a folding (θ) of the MS_2C_2 metallacycle along the S−S axis upon oxidation to the d^1 paramagnetic cation. The evolution of the peculiar unfolded structure ($\theta = 0°$) of $Cp_2Mo(dmit)^{\bullet+}$ ($dmit^{2-}$, 2-thioxo-1,3-dithiole-4,5-dithiolate) in its AsF_6^- salt toward the introduction of heavy atoms (W, Se) is examined here by substituting $dsit^{2-}$ ($dsit^{2-}$, 2-thioxo-1,3-dithiole-4,5-diselenolate) for $dmit^{2-}$ and/or W for Mo in those AsF_6^- salts. While $[Cp_2Mo(dsit)^{\bullet+}][AsF_6^-]$ (orthorhombic, *Cmcm*, $a = 9.071(2)$, $b = 20.868(4)$, $c = 10.243(2)$ Å, $V = 1938.9(7)$ Å^3, $Z = 4$) and $[Cp_2W(dmit)^{\bullet+}][AsF_6^-]$ (orthorhombic, *Cmcm*, $a = 9.0295(15)$, $b = 20.568(2)$, $c = 10.2641(12)$ Å, $V = 1906.2(4)$ Å^3, $Z = 4$) crystallize with an unfolded geometry and are isostructural with $[Cp_2Mo(dmit)^{\bullet+}][AsF_6^-]$, the introduction of both W and $dsit^{2-}$ in $Cp_2W(dsit)$ stabilizes a fully different structure for $[Cp_2W(dsit)^{\bullet+}][AsF_6^-]$ (monoclinic, $P2_1/c$, $a = 6.8442$, $b = 15.9923(13)$, $c = 17.6594(16)$ Å, $\beta = 90.934(11)°$, $V = 1932.6(3)$ Å^3, $Z = 4$) with the $Cp_2W(dsit)^{\bullet+}$ cation in a folded geometry ($\theta = 30.1(1)°$). DFT calculations show that the variety of folding angles and hence of molecular structures found in those open-shell d^1 Cp_2M(dithiolene)$^{\bullet+}$ complexes is attributable to a very low energy cost (<1 kcal mol^{-1}) for folding around the minimal energy folding angle. The molecular geometry of those complexes and hence their frontier orbitals are therefore highly related to the actual crystal structure they adopt. The unfolded complexes exhibit, in their AsF_6^- salts, a three-dimensional set of intermolecular interactions in the solid state, confirmed by the presence of an antiferromagnetic ground state ($T_{Néel} = 3.5(5)$ K in $[Cp_2W(dmit)^{\bullet+}][AsF_6^-]$). On the other hand, the folding of $Cp_2W(dsit)^{\bullet+}$ in $[Cp_2W(dsit)^{\bullet+}][AsF_6^-]$ leads to the formation of a rare spin-ladder system with a spin gap of 90−100 K, as deduced from the temperature dependence of its magnetic susceptibility.

Introduction

Molybdenum (tungsten) dithiolene complexes raise a particular interest as models of metalloenzymes such as the molybdenum cofactors,[2] since several recent protein crystal structures highlighted the general figure of a metal atom in its (IV) or (VI) oxidation state[3] and coordinated by one or two dithiolene ligands appended to a tricyclic pyranopterin, confirming the structure anticipated by Rajagopalan in 1980.[4] The subtle conformational modifications which have been identified accompanying redox changes of the enzymes[5] illustrate the crucial role of the "noninnocent" dithiolene ligand in the processes involved in the enzyme's catalytic cycle. Of the utmost importance is therefore the relationship between the metal coordination sphere, its electronic structures, and how changes in both relate to the catalytic activity. In that respect, the most detailed information about the electronic structure of the Mo centers can be obtained from studies of the paramagnetic Mo(V) state, by EPR/ENDOR studies[6] or in model compounds,[7,8] while the Mo(IV) or Mo(VI) states are most easily generated for protein crystallography.[3] The evaluation of the structural similarity of the Mo(V) state with either the Mo(IV) or the Mo(VI) states would allow for a clearer description of the electronic structure of the metal center (coordination sphere, HOMO, LUMO) and the possible electronic pathways for electron transfer. In that respect we recently demonstrated that mixed Mo(IV) cyclopentadienyl/dithiolene complexes of general formula $Cp_2Mo(dithiolene)$[9] (Scheme 1) or $Cp^*Mo(dithiolene)_2^{1-}$,[10] with one or two dithiolene ligands in the coordination sphere of the metal, were able to sustain reversible oxidation to the Mo(V) and Mo(VI) states and several Mo(V) complexes were accordingly crystallographically characterized. Their main fea-

(1) (a) Institut des Matériaux Jean Rouxel. (b) Centre de Recherches Paul Pascal.
(2) (a) Holm, R. H.; Kennepohl, P.; Solomon, E. I. *Chem. Rev.* **1996**, *96*, 2239. (b) Hille, R. *Chem. Rev.* **1996**, *96*, 2757. (c) Collison, D.; Garner, C. D.; Joule, J. A. *Chem. Soc. Rev.* **1996**, *25*, 25.
(3) (a) Romao, R. J.; Archer, M.; Moura, I.; Moura, J. J. G.; LeGall, J.; Engh, R.; Schneider, M.; Hof, P.; Huber, R. *Science* **1995**, *270*, 1170. (b) Schindelin, H.; Kisker, C.; Hilton, J.; Rajagopalan, K. V.; Rees, D. C. *Science* **1996**, *272*, 1615. (c) Schneider, F.; Löwe, J.; Huber, R.; Schindelin, H.; Kisker, C.; Knäblein, J. *J. Mol. Biol.* **1996**, *263*, 53. (d) Boyington, J. C.; Gladyshev, V. N.; Khangulov, S. V.; Stadtman, T. C.; Sun, P. D. *Science* **1997**, *275*, 1305.
(4) (a) Johnson, J. L.; Hainline, B. E.; Rajagopalan, K. V. *J. Biol. Chem.* **1980**, *255*, 1783. (b) Garrett, R. M.; Rajagopalan, K. V. *J. Biol. Chem.* **1996**, *271*, 7387 and references therein.
(5) Schindelin, H.; Kisker, C.; Rees, D. C. *J. Biol. Inorg. Chem.* **1997**, *2*, 773.
(6) Pacheco, A.; Basu, P.; Borbat, P.; Raitsimring, A. M.; Enemark, J. H. *Inorg. Chem.* **1996**, *35*, 7001.
(7) Davies, E. S.; Beddoes, R. L.; Collison, D.; Dinsmore, A.; Docrat, A.; Joule, J. A.; Wilson, C. R.; Garner, C. D. *J. Chem. Soc., Dalton Trans.* **1997**, 3985.
(8) (a) Kaiwar, S. P.; Hsu, J. K.; Vodacek, A.; Yap, G.; Liable-Sands, L. M.; Rheingold, A. L.; Pilato, R. S. *Inorg. Chem.* **1997**, *36*, 2406, (b) Hsu, J. K.; Bonangelino, C. J.; Kaiwar, S. P.; Boggs, C. M.; Fettinger, J. C.; Pilato, R. S. *Inorg. Chem.* **1996**, *35*, 4743.
(9) Fourmigué, M.; Lenoir, C.; Coulon, C.; Guyon, F.; Amaudrut, J. *Inorg. Chem.* **1995**, *34*, 4979.
(10) Fourmigué, M.; Coulon, C. *Adv. Mater.* **1994**, *6*, 948.

10.1021/ic000550y CCC: $20.00
Published on Web 12/16/2000

Scheme 1

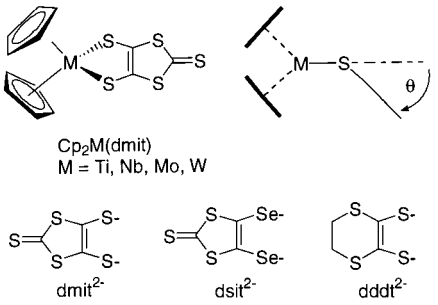

ture lies in a possible folding of the MoS_2C_2 metallacycle along the S−S axis, a metallacycle which is almost flat in the Mo(IV) complexes and appears to be bent to some extent upon oxidation to the Mo(V) state.

This behavior was rationalized some years ago by Lauher and Hoffmann[11] on the basis of extended Hückel calculations on d^0 Ti(IV) and d^2 Mo(IV) complexes of general formula $Cp_2M(dithiolene)$,[12] demonstrating that the strong folding of the d^0 titanium species ($40° < \theta < 50°$) found its origin in the overlap stabilization of the empty metallic and occupied dithiolene frontier orbitals, of a_1 and b_1 symmetry respectively, hindering any mixing in the unfolded C_{2v} conformation ($\theta = 0°$) but affording a net stabilization in the folded C_s conformation ($\theta > 0$). The two extra electrons of the d^2 Mo(IV) complexes would occupy the antibonding combination of both fragment orbitals, hence the absence of folding. The situation of the d^1 species was not addressed at that time, and only a few complexes were reported with intermediate folding angle values ($30° < \theta < 40°$), as 38.3° in $Cp_2V(o\text{-}S_2C_6H_4)$,[13] 34° in $Cp'_2Nb(dmit)$[14] ($dmit^{2-}$: 2-thioxo-1,3-dithiole-4,5-dithiolate), and 32.3° in the cationic Mo(V) $[Cp_2Mo(dddt)]^{\bullet+}$.[9]

We have shown in a previous paper[15] that six different d^1 $Cp_2M(dithiolene)^{\bullet+}$ complexes, in their 1:1 salts with $TCNQF_4^{\bullet-}$, $[Cp_2M(dithiolene)^{\bullet+}][TCNQF_4^{\bullet-}]$, exhibited a large range of folding angles of the metallacycle along the S−S axis which were not restricted between 30 and 40° but vary from 10° in $Cp_2Mo(dmit)^{\bullet+}$ up to 32.38(1)° in $Cp_2W(dsit)^{\bullet+}$ ($dsit^{2-}$: 2-thioxo-1,3-dithiole-4,5-diselenolate), depending upon the nature of the metal (Mo vs W) and the dithiolene ($dmit^{2-}$ vs $dmid^{2-}$ vs $dsit^{2-}$; $dmid^{2-}$, 2-oxo-1,3-dithiole-4,5-dithiolate), the strongest folding being observed with the heaviest elements (W, Se). Also, we have recently described a series of salts of $Cp_2Mo(dmit)^{\bullet+}$ with PF_6^-, AsF_6^-, and SbF_6^- where surprisingly the Mo(V) oxidized complexes were not folded at all: $\theta = 0°$![16] The question then arises if the absence of folding in these oxidized complexes represents a true energy minimum for the system or is the consequence of the peculiar crystal structure of the $[Cp_2Mo(dmit)^{\bullet+}][XF_6^-]$ salts, X = P, As, Sb. This is all the more questionable since those salts were shown to exhibit, upon cooling, first- and second-order structural transitions which might suggest an intrinsic instability of this highly symmetrical molecular structure with $\theta = 0°$.[16]

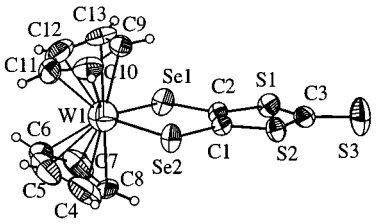

Figure 1. ORTEP view and numbering scheme of $Cp_2W(dsit)$ with 50% probability displacement ellipsoids.

We therefore undertook to "test" the resistance of this unfolded conformation to different stresses by changing the nature of the organometallic cation and substituting W and/or $dsit^{2-}$ for Mo and $dmit^{2-}$ in $[Cp_2Mo(dmit)^{\bullet+}][AsF_6^-]$ to evaluate how these substitutions would affect this surprising unfolded molecular structure and, as inferred from our previous results with the $TCNQF_4^{\bullet-}$ salts,[15] eventually lead to a folded metallacycle and a novel solid state structure. We accordingly prepared the AsF_6^- salts of the three $Cp_2Mo(dmit)$ analogues, i.e., $Cp_2Mo(dsit)$, $Cp_2W(dmit)$, and $Cp_2W(dsit)$, to compare the molecular structure of the complexes upon these different substitutions in the same crystallographic environment. The structural and magnetic properties of these salts will be compared with those of the parent $[Cp_2Mo(dmit)^{\bullet+}][AsF_6^-]$ salt. Furthermore, although the extended Hückel analysis firmly rationalized the unfolded conformation of the d^2 complexes and highly folded conformation of the d^0 complexes, the precise structural properties of the open-shell d^1 complexes were not amenable by this method.

We therefore performed geometry optimizations of the four $Cp_2M(dithiolene)$ complexes (M = Mo, W, dithiolene = $dmit^{2-}$, $dsit^{2-}$) in their neutral (d^2) and oxidized (d^1) forms using DFT calculations, to obtain the energy profile of the folding process and give a rationale for the observed differences between the four oxidized complexes. This analysis of the structural evolutions on the one hand and the outcome of the theoretical calculations on the other hand are expected to bring some insight into the precise requirements which govern the organization of the dithiolene ligands in the coordination sphere of the metal, in its V oxidation stage.

Results and Discussion

The Neutral Complexes and Their Electrocrystallization. The four $Cp_2M(dithiolene)$ (M = Mo, W; dithiolene = $dmit^{2-}$, $dsit^{2-}$) complexes were prepared as previously described.[15] The X-ray crystal structures of the neutral, unoxidized $Cp_2Mo(dmit)$, and $Cp_2W(dsit)$ were also determined in order to compare their structural characteristics (bond lengths, bond angles, folding) with those of the oxidized complexes. $Cp_2Mo(dmit)$ and $Cp_2W(dsit)$ are isostructural and crystallize in the monoclinic system, space group *C*2/*c* (Figure 1). The molecules are located in a general position in the unit cell; important bond distances and angles are collected in Table 1. Note that in both complexes the metallacycle is nearly planar with folding angles (θ) values close to 0°, i.e., 4.2(1)° in $Cp_2Mo(dmit)$ and 4.5°(5)° in $Cp_2W(dsit)$, as expected for d^2 Mo[17,18] or W complexes.[19]

(11) Lauher, J. W.; Hoffmann, R. *J. Am. Chem. Soc.* **1976**, *98*, 1729.
(12) Fourmigué, M. *Coord. Chem. Rev.* **1998**, *178*−*180*, 823.
(13) Stephan, D. W. *Inorg. Chem.* **1992**, *31*, 4218.
(14) Cp′, η^5-$C_5H_4SiMe_3$; Guyon, F.; Fourmigué, M.; Clérac, R.; Amaudrut, J. *J. Chem. Soc., Dalton Trans.* **1996**, 4093.
(15) Fourmigué, M.; Domercq, B.; Jourdain, I. V.; Molinié, P.; Guyon, F.; Amaudrut, J. *Chem. Eur. J.* **1998**, *9*, 1714.
(16) (a) Clérac, R.; Fourmigué, M.; Gaultier, J.; Barrans, Y.; Albouy, P. A.; Coulon, C. *Eur. Phys. J. B* **1999**, *9*, 431. (b) Clérac, R.; Fourmigué, M.; Gaultier, J.; Barrans, Y.; Albouy, P. A.; Coulon, C. *Eur. Phys. J. B* **1999**, *9*, 445.
(17) (a) Knox, J. R.; Prout, C. K. *J. Chem. Soc., Chem. Commun.* **1967**, 1277. (b) Kutoglu, A.; Köpf, H. *J. Organomet. Chem.* **1970**, *25*, 455.
(18) (a) Hsu, J. K.; Bonangelino, C. J.; Kaiar, S. P.; Boggs, C. M.; Fettinger, J. C.; Pilato, R. S. *Inorg. Chem.* **1996**, *36*, 4743. (b) Pilato, R. S.; Eriksen, K. A.; Greaney, M. A.; Stiefel, E. I. *J. Am. Chem. Soc.* **1991**, *113*, 9372.
(19) Debaerdemaeker, T.; Kutoglu, A. *Acta Crystallogr.* **1973**, *B29*, 2664.

Table 1. Calculated (DFT) and Experimental (X-ray) Geometrical Characteristics of the Neutral Cp_2M(dithiolene) Complexes (Q = S in $dmit^{2-}$, Q = Se in $dsit^{2-}$)

		$Cp_2Ti(dmit)^a$	$Cp_2Nb(dmit)^b$	$Cp_2Mo(dmit)$	$Cp_2Mo(dsit)$	$Cp_2W(dmit)$	$Cp_2W(dsit)$
M−Q (Å)	calc	2.493	2.561	2.498	2.605	2.490	2.599
	X-ray	2.431(2)	2.51(2)	2.457(3)			2.578(9)
Q−C (Å)	calc	1.792	1.812	1.820	1.948	1.828	1.956
	X-ray	1.72(1)	1.78(5)	1.745(9)			1.903(8)
C═C (Å)	calc	1.394	1.380	1.366	1.366	1.363	1.363
	X-ray	1.358(2)	1.25(3)	1.357(12)			1.343(10)
Q−M−Q (deg)	calc	84.32	82.40	84.04	84.68	84.31	84.97
	X-ray	84.40(2)	81.3(6)	83.95(8)			85.00(3)
θ (deg)	calc	46.1	32.6	0	0	0	0
	X-ray	47.4	34	4.2(1)			4.50(5)

[a] Experimental X-ray data are taken from ref 21. [b] Experimental X-ray data are taken from ref 14.

Table 2. Calculated (DFT) and Experimental (in the AsF_6^- Salts) Geometrical Characteristics of the Open-shell $Cp_2M(dithiolene)^{\bullet+}$ Complexes (Q = S in $dmit^{2-}$, Q = Se in $dsit^{2-}$)[a]

		$Cp_2Mo(dmit)^{\bullet+}$ [b]	$Cp_2Mo(dsit)^{\bullet+}$	$Cp_2W(dmit)^{\bullet+}$	$Cp_2W(dsit)^{\bullet+}$
M−Q (Å)	calc	2.529	2.631	2.512	2.616
	X-ray	2.441(2) [−0.6%]	2.559(1)	2.429(1)	2.545(11) [−1.3%]
Q−C (Å)	calc	1.788	1.917	1.796	1.924
	X-ray	1.691(8) [−3.1%]	1.837(8)	1.693(5)	1.872(6) [−1.6%]
C═C (Å)	calc	1.402	1.399	1.397	1.395
	X-ray	1.41(1) [+3.9%]	1.37(2)	1.384(9)	1.362(8) [+1.4%]
Q−M−Q (deg)	calc	83.21	84.12	83.28	84.16
	X-ray	83.59(8)	84.74(5)	83.86(7)	83.75(2)
θ (deg)	calc	14.12	14.39	21.59	22.57
	X-ray	0	0	0	30.1(1)

[a] In square brackets are given the bond length variations relative to the structures of the unoxidized neutral complexes (see Table 1) showing the increased dithioketonic character of the ligand upon oxidation. [b] Experimental data are taken from ref 16a.

The electrocrystallization of $Cp_2Mo(dmit)$ in the presence of n-Bu_4NAsF_6 was reported[16] to afford the 1:1 salt [$Cp_2Mo(dmit)^{\bullet+}$][AsF_6^-], as elongated plates, crystallizing in the orthorhombic system, space group *Cmcm*, with the cation in a fully unfolded conformation ($\theta = 0°$). The determination (see above) of the X-ray crystal structure of the neutral $Cp_2Mo(dmit)$ allows now a comparison of the bond lengths between the neutral molecule and oxidized molecule (Table 2). The Mo−S bond remains nearly constant upon oxidation (small shortening) while the C−S bonds exhibit a marked shortening with a concurrent lengthening of the C═C double bond, demonstrating unambiguously that the oxidation process markedly affects the dithiolene moiety, which adopts a dithioketonic character.[9] This behavior is in agreement with the nature of the HOMO of $Cp_2Mo(dmit)$ determined by molecular orbital calculations (vide infra), with a frontier orbital essentially localized on the dithiolene fragment.

Under the same conditions, if we now substitute the tungsten for the molybdenum, the electrocrystallization of $Cp_2W(dmit)$ affords crystals of similar shape whose X-ray crystal structure determination shows that they are isostructural with the molybdenum complex. They crystallize in the orthorhombic system, space group *Cmcm*, with $a = 9.0295(15)$, $b = 20.568(2)$, $c = 10.2641(12)$ Å, and $V = 1906.2(4)$ Å^3. The $Cp_2W(dmit)^{\bullet+}$ is located at the crossing of the two mirror planes, in the *m*2*m* site (Figure 2), and as a consequence, the metallacycle is similarly unfolded. Bond distances and angles are very close to those observed in [$Cp_2Mo(dmit)^{\bullet+}$][AsF_6^-] (Table 2), with the W−S bond only slightly shorter than the Mo−S one. Within this structure, we have shown that each open-shell cation interacts through three different interactions with 10 neighboring molecules, affording a three-dimensional interaction network, as observed in [$Cp_2Mo(dmit)^{\bullet+}$][AsF_6^-].[16] Extended Hückel calculations of the three corresponding HOMO−HOMO intermolecular interaction energies (49, 35, and 22 meV) are very close to those determined in [$Cp_2Mo(dmit)^{\bullet+}$][AsF_6^-] (44, 33, and 24 meV). In conclusion, the crystallization of [$Cp_2W(dmit)^{\bullet+}$][AsF_6^-] within this orthorhombic structure demonstrates that the Mo/W exchange does not introduce a sufficient strain on the molecule to induce its folding and an accompanying structural change.

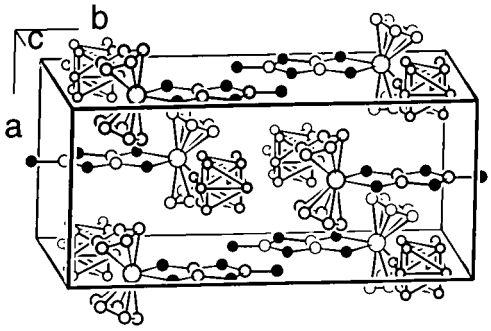

Figure 2. View of the orthorhombic unit cell of the AsF_6^- salts of $Cp_2Mo(dmit)$, $Cp_2Mo(dsit)$, and $Cp_2W(dmit)$. Note the unfolded conformation ($\theta = 0°$) of the d^1 cationic complexes.

If we now substitute the *dithiolene* ligand in $Cp_2Mo(dmit)$ and consider the electrocrystallization of $Cp_2Mo(dsit)$ under the same conditions, crystals hardly grow on the electrode. Increasing the current density or decreasing the temperature did not improve the crystal quality, and only a few plates were obtained upon cooling of the electrocrystallized solutions. X-ray crystal structure determination shows them to be isostructural with the [$Cp_2Mo(dmit)^{\bullet+}$] and the [$Cp_2W(dmit)^{\bullet+}$] salts. [$Cp_2Mo(dsit)^{\bullet+}$][AsF_6^-] crystallizes in the orthorhombic system, space group *Cmcm*, with $a = 9.071(2)$, $b = 20.868(4)$, $c = 10.243(2)$ Å, and $V = 1938.9(7)$ Å^3 with the $Cp_2Mo(dsit)^{\bullet+}$ cation on the *m*2*m* site in the unfolded conformation ($\theta = 0°$). Characteristic bond lengths and angles are collected in Table 2. The difficulties encountered with the crystallization of this salt show, however, that the $dsit^{2-}$ ligand either gives a higher solubility which

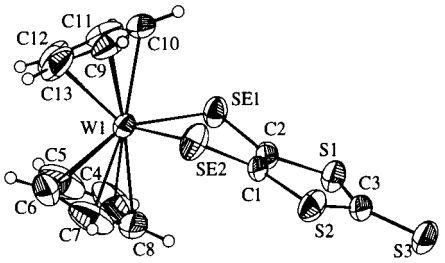

Figure 3. ORTEP view and numbering scheme of $Cp_2W(dsit)^{\bullet+}$ in $[Cp_2W(dsit)^{\bullet+}][AsF_6^-]$ with 50% probability displacement ellipsoids.

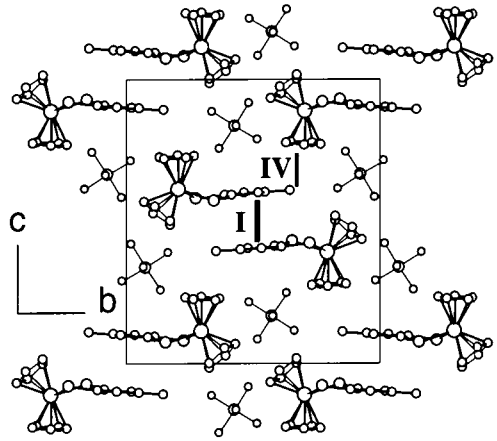

Figure 4. Projection view of $[Cp_2W(dsit)^{\bullet+}][AsF_6^-]$ along *a* showing the solid-state organization of the open-shell cationic $Cp_2W(dsit)^{\bullet+}$ complexes within dimers (interaction I).

hinders the proper precipitation of the orthorhombic phase or introduces an electronic interaction which does not favor the precipitation of this phase.

In that respect, if we now replace *both* the metal *and* the ligand in $Cp_2Mo(dmit)$ and substitute the tungsten for the molybdenum *and* the $dsit^{2-}$ for the $dmit^{2-}$, the electrocrystallization of $Cp_2W(dsit)$ under the usual conditions afforded needlelike high-quality crystals which no longer belong to the isostructural orthorhombic series found above: $[Cp_2W(dsit)^{\bullet+}][AsF_6^-]$ crystallizes in the monoclinic system, space group $P2_1/c$ with $a = 6.8442(7)$, $b = 15.992\ (1)$, $c = 17.659(2)$ Å, $\beta = 90.93(1)°$, and $V = 1932.6(3)$ Å^3. The organometallic cation (Figure 3) is located in a general position in the unit cell, and its most striking feature is its strong folding, 30.1(1)°. Comparison of the bond lengths (Table 2) within the organometallic cation with those of the neutral molecule $Cp_2W(dsit)$ shows that the diselenolene moiety also adopts a diselenoketonic structure upon oxidation with a shortening of the C−Se bonds and lengthening of the central C=C double bond while the W−Se bond shortens slightly, an indication of a somewhat stronger W/dsit bonding interaction in the oxidized $Cp_2W(dsit)^{\bullet+}$ organometallic cation.

This folded molecular geometry has important consequences for the solid-state structure adopted by $[Cp_2W(dsit)^{\bullet+}][AsF_6^-]$. As shown in Figure 4, the cations are no longer arranged into a three-dimensional array but are rather associated into inversion-related dimers with two intradimer Se2···S2^{i} distances[20] at 3.716(1) Å (i: $1 - x, -y, -z$; interaction I). Those dimers interact with each other along the *a* direction (Figure 5) with short interdimer chalcogene−chalcogene contacts of Se2···Se1^{ii}

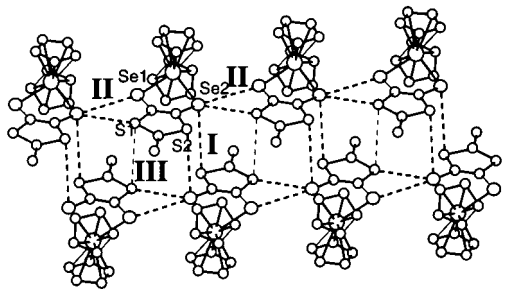

Figure 5. View of the ladder-type organization of the dimers in $[Cp_2W(dsit)^{\bullet+}][AsF_6^-]$ with interactions I, II, and III.

3.812(1) Å, and Se2···S1^{ii} 3.495(4) Å (ii: $1 + x, y, z$; interaction II), giving rise to a ladderlike solid-state organization. Other intermolecular contacts are also identified, within the ladder with S1···S1^{iii} at 3.690(5) Å (iii: $1 - x, -y, -z$; interaction III in Figure 5) and between the ladders through a cyclopentadiene/dsit contact with S3···C6^{iv} 3.64(1) Å (iv: $1 - x, -0.5 + y, 0.5 - z$; interaction IV in Figure 4). We observe at this stage of our work that the introduction of both the tungsten *and* the dsit ligand was necessary to finally bring about the collapse of the orthorhombic structure with $\theta = 0°$ and the setting of a folded metallacycle and a novel ladderlike structure. While the three other complexes, $Cp_2Mo(dmit)^{\bullet+}$, $Cp_2Mo(dsit)^{\bullet+}$, and $Cp_2W(dmit)^{\bullet+}$ are able to adopt, depending upon the nature of the counteranion ($TCNQF_4^{\bullet-}$,[15] AsF_6^-) and a wide range of conformations with θ varying between 0° and 35°, $Cp_2W(dsit)^{\bullet+}$ appears to be strongly reluctant to crystallize in the unfolded conformation. DFT calculations were therefore performed on those complexes to possibly understand the origin of the high flexibility encountered with the first three complexes and the apparently peculiar character of $Cp_2W(dsit)^{\bullet+}$.

The Energy Profile of the Folding Process. DFT calculations were first performed on model systems in order to validate the method and the parameters we used, i.e., on the highly folded ($\theta = 47.4(3)°$) diamagnetic (d^0) $Cp_2Ti(dmit)$ complex,[21] the paramagnetic d^1 $Cp'_2Nb(dmit)$ complex[14] with $\theta = 34°$, and of course the four neutral d^2 $Cp_2M(dithiolene)$ complexes with observed θ values close to 0°. The geometry optimizations performed with those complexes converged toward geometries very close to those determined by X-ray diffraction (Table 1). While the calculated bond distances are systematically found slightly longer (around +3%) than the experimental ones, bond angles and, most significantly here, the folding angle of the metallacycle are found in very close agreement with the experimental ones, confirming the extended Hückel analysis developed earlier by Lauher and Hoffmann.[11] The introduction of polarizing orbitals (6-31G**) for the chalcogen atoms does not significantly improve the metal−chalcogen bond lengths. An energy scan of the folding in $Cp_2Ti(dmit)$ was also performed by calculating the total energy of the system while imposing different folding angles around the minimum energy angle found in the geometry optimization (46.1°; X-ray 47.4(3)°).[21] As shown in Figure 6, a deep energy well is found with a calculated barrier for inversion around 15 kcal mol^{-1}, a value in very good agreement with that determined experimentally from variable-temperature NMR experiments at 14 kcal mol^{-1}.[21] The geometry optimizations performed on the open-shell d^1 complex $Cp'_2Nb(dmit)$ also converged to a geometry in very good agreement with the experimental data, for instance a calculated folding angle of 32.6° (X-ray 34°).[14] Note also that

(20) The sum of the van der Waals radii for Se···Se and Se···S contacts are 3.80 and 3.70 Å, respectively: Bondi, A. *J. Phys. Chem.* **1964**, *68*, 441.

(21) Guyon, F.; Lenoir, C.; Fourmigué, M.; Larsen, J.; Amaudrut, J. *Bull. Soc. Chim. Fr.* **1994**, *131*, 217.

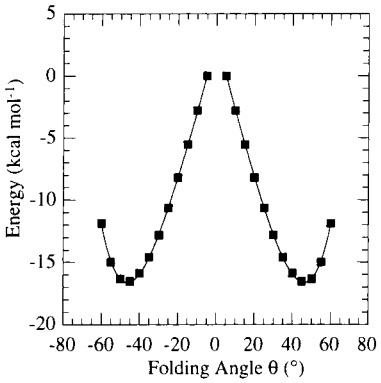

Figure 6. Energy scan of the folding process in the $d^0Cp_2Ti(dmit)$.

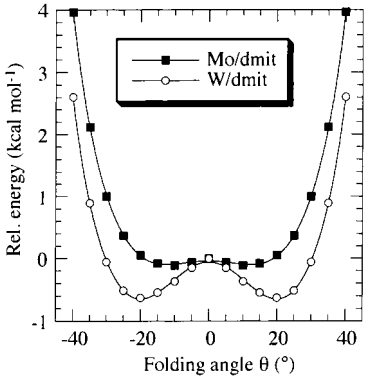

Figure 7. Energy scan of the folding process in the d^1 $Cp_2Mo(dmit)^{\bullet+}$ and $Cp_2W(dmit)^{\bullet+}$.

the geometry optimization of the Mo and W complexes, initially started in C_s geometry with $\theta \neq 0°$, systematically converged toward $\theta = 0°$; the optimization was therefore completed in C_{2v} geometry with an imposed $\theta = 0°$ constraint.

It is therefore with a good degree of confidence that we tackled the same geometry optimizations of the four open-shell $Cp_2M(dithiolene)^{\bullet+}$ complexes. Results are collected in Table 2, and optimized bond lengths and angles are compared with those found in the X-ray crystal structures of the AsF_6^- salts described here. As already observed above with neutral d^0, d^1, and d^2 complexes (Table 1), calculated bond distances are systematically found slightly longer than those measured experimentally while bond angles are reproduced very well. The increased dithioketonic character of the ligand, experimentally observed (see above) upon oxidation, is well reproduced by the calculations. On the other hand, the metal−chalcogen bond length is predicted to increase upon oxidation in the four complexes while it slightly decreases in the crystal structures of the four AsF_6^- salts. If we now analyze the differences found in the calculated geometries of the four oxidized complexes, particularly the predicted folding angles (Table 2), it is clear that the predicted angles for the molybdenum complexes ($\theta \approx 14°$) are indeed smaller than that for tungsten complexes ($\theta \approx 22°$). Surprisingly, the nature of the dithiolene ligand does not seem to influence the calculated folding angle, in apparent contradiction to the differences observed between the two tungsten salts with either the dmit or the dsit ligands. A deeper understanding of this behavior is given by the energy scan of the folding performed for the four cations as described above for $Cp_2Ti(dmit)$.

The two representative examples of $Cp_2Mo(dmit)$ and $Cp_2W(dmit)$ are given in Figure 7. Indeed, as already observed during the geometry optimization, the nature of the dithiolene does not

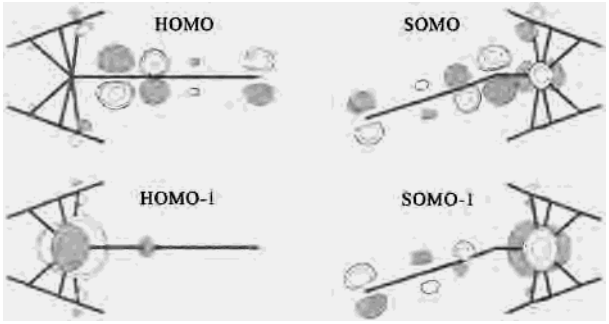

Figure 8. Representations of the HOMO and HOMO-1 of $Cp_2Mo(dmit)$ ($\theta = 0°$) and the SOMO and SOMO-1 of the $Cp_2W(dsit)^{\bullet+}$ cation ($\theta = 30.1°$).

modify the general figure, both Mo complexes behave similarly, as do both W complexes. Note also that whatever the nature of the metal or the dithiolene, the energy wells are *very shallow* (<0.5 kcal mol^{-1}) and every complex, even $Cp_2W(dsit)$ with the heaviest atoms, is expected to adopt every possible geometry with θ between 0° and 35° without exceeding an energy cost of 1 kcal mol^{-1}. This very peculiar behavior of the d^1 complexes gives a clue to the observed versatility of molecular structures encountered with those highly flexible cationic species. It also demonstrates that the molecular structure adopted by the organometallic complexes is largely correlated with the nature, shape, and symmetry of the counteranion, an original feature of those complexes. Furthermore, as shown in Figure 8, the folding of the complexes also induces a specific distribution in the SOMO between the metal and the dithiolene moieties: unfolded complexes concentrate their SOMO on the dithiolene fragment while an increased folding of the metallacycle leads to a decreased spin density on the dithiolene with a concurrent increase on the Cp_2M fragment. This effect was already noted in the analysis of the bond length evolution upon oxidation and is further substantiated by the fact that the largest bond length variations within the dithiolene moiety (Table 2) are indeed observed in the unfolded complexes where the C−Q and C═C bonds change by 3%−4% while only 1.5% variations are observed in the folded complex. We are therefore faced here with molecules whose HOMO is potentially different for every given crystal structure, a very rare example of combined structural and electronic versatility in molecular engineering. As a consequence, different folding angles correlated with different crystal structures are expected to also bring about different intermolecular interaction networks and accordingly different solid-state magnetic properties.

From the 3D Antiferromagnet to the Spin Ladder. The three-dimensional set of intermolecular interactions observed in $[Cp_2Mo(dmit)^{\bullet+}][AsF_6^-]$ led this salt to order antiferromagnetically for $T < T_{Néel} = 9.5(5)$ K after two second-order transitions observed at 142 and 61 K.[16] It was also shown that the substitution of the smaller PF_6^- or larger SbF_6^- anions for the AsF_6^- anion had a deep influence on those structural transitions which precede the antiferromagnetic ordering. It is therefore of interest to investigate and compare the magnetic properties of the two isostructural orthorhombic phases described here involving $[Cp_2W(dmit)^{\bullet+}]$ and $[Cp_2Mo(dsit)^{\bullet+}]$ with those of the $[Cp_2Mo(dmit)^{\bullet+}]$ salt. In the following we will restrain ourselves to $[Cp_2W(dmit)^{\bullet+}][AsF_6^-]$ since the $[Cp_2Mo(dsit)^{\bullet+}]$ salt was obtained in very small quantities only. The temperature dependence of the susceptibility of $[Cp_2W(dmit)^{\bullet+}][AsF_6^-]$ (Figure 9) follows a Curie−Weiss law in the high-temperature regime with $\theta_{Weiss} = -3.4(5)$ K and exhibits a saturation at the lowest temperatures. Below 3.5 K, the salt undergoes a transition

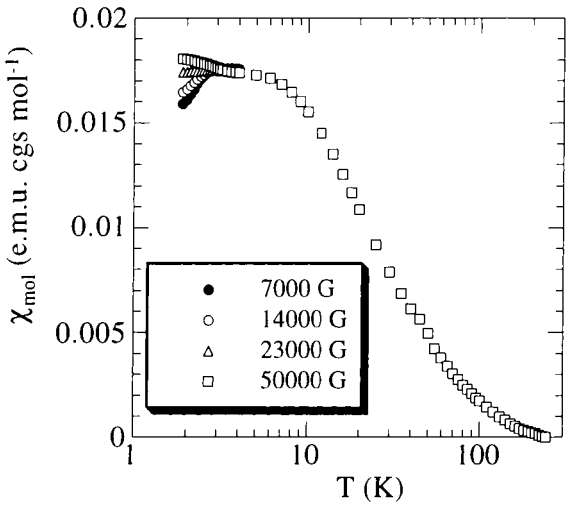

Figure 9. Temperature dependence of the magnetic susceptibility of $[Cp_2W(dmit)^{\bullet+}][AsF_6^-]$. The field dependence of the susceptibility is shown at low temperature.

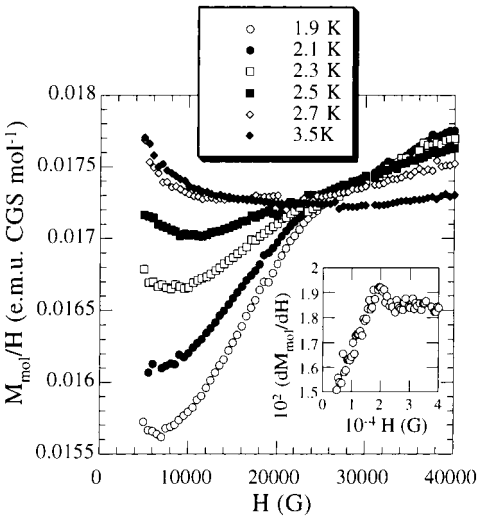

Figure 10. Field dependence of M_{mol}/H at different temperatures below $T_{Néel}$. Insert: the maximum of $(\partial M_{mol}/\partial H_{1.9\ K})$ vs H gives the spin-flop field of 19 000 G.

to an antiferromagnetic ground state, as shown by the field dependence of the susceptibility. This value of $T_{Néel} = 3.5(5)$ K is compatible with the θ_{Weiss} determined above. The field dependence of the magnetic susceptibility below $T_{Néel}$ has been investigated in detail (Figure 10) at different temperatures and confirms the presence of an antiferromagnetic ground state. The slight increase of susceptibility at the lowest fields (5000−7000 G) is attributable to a very small amount of ferromagnetic impurities. According to Uyeda and Date,[22] who determined, in the frame of the mean-field Nagamiya theory of two-sublattice antiferromagnetism (AF), the susceptibility of a powder sample in the AF state, we deduce the spin−flop field (H_{SP}) value of 19 000 G from the maximum of $\partial M_{mol}/\partial H = f(H)$ (Figure 10, insert).[23] Note that the ratio of the lowest-field to the highest-field values of $\partial M_{mol}/\partial H$ at the lowest temperature (1.9 K) amounts to 0.83 while a value of 2/3 is predicted at 0 K. This ratio which writes as $1 - r/3$ where $r = 1 - \chi_{\parallel}/\chi_{\perp}$ gives a $r_{1.9\ K}$ value of 0.51. According to the Nagamiya mean-field theory, the r value is related to $T/T_{Néel}$ and gives a Néel temperature of

(22) Uyeda, C.; Date, M. *J. Phys. Soc. Jpn.* **1986**, *55*, 2830.
(23) Clérac, C. Ph.D. Thesis, University of Bordeaux I, France, 1997.

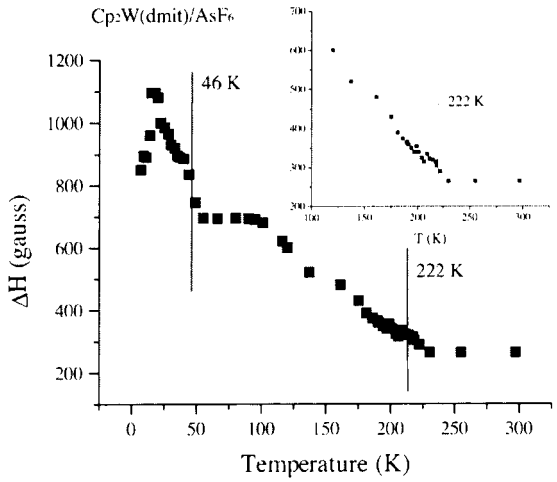

Figure 11. Temperature dependence of the ESR line width in $[Cp_2W(dmit)^{\bullet+}][AsF_6^-]$. Detail of the 222 K transition is given in the insert.

3.2 K, in good agreement with the Néel temperature determined above. Of particular note is also the field dependence at higher fields ($H > H_{SP}$), which is specific to the AF ground state since it is not observed at 3.5 K but is not predicted in a mean-field theory. We do not have a definitive explanation for such a field evolution (approximately as $a + bH^2$) which is also observed in other molecular antiferromagnetic systems.[23] Those values of θ_{Weiss}, $T_{Néel}$, and H_{SP} are to be compared with those reported for the molybdenum salt where the antiferromagnetic interactions appear stronger ($\theta_{Weiss} = -21$ K, $T_{Néel} = 9.5$ K) but the spin−flop appears field much smaller (6500 G). While the higher H_{SP} value of the tungsten complex can be attributed to the stronger effect of the spin−orbit coupling, the close proximity of the θ_{Weiss} and $T_{Néel}$ values in $[Cp_2W(dmit)^{\bullet+}][AsF_6^-]$ would indicate a more isotropic set of intermolecular interactions, a result in contradiction to its structure where the substitution of the tungsten for the molybdenum introduces extremely weak modifications mainly attributable to the shortening of the W−S bond when compared with the Mo−S one.

In single-crystal EPR experiments, one single line is observed, whose anisotropy ($g_a = 2.001$, $g_b = 2.025$, $g_c = 2.011$) is close to that observed in the molybdenum salt ($g_a = 1.9999$, $g_b = 2.0276$, $g_c = 2.0133$), confirming that the spin density is preferentially localized on the dithiolene moiety. On the other hand, the room-temperature line width (Figure 11) is much larger and highly anisotropic ($\Delta H_a = 270$ G, $\Delta H_b = 400$ G, $\Delta H_c = 325$ G). Those results also indicate that the stronger spin−orbit coupling in the tungsten salt plays an important role in the spin dynamics, in both the paramagnetic regime (ΔH increase) and the antiferromagnetic regime (H_{SP} increase), which might explain the smaller $T_{Néel}$ temperature observed in this salt. Furthermore, the hypothesis that this orthorhombic structure with an unfolded metallacycle would be more unstable in the presence of heavy atoms is further substantiated by the temperature dependence of the EPR line width. As shown in Figure 11, the first structural transition which was detected at 142 K in $[Cp_2Mo(dmit)^{\bullet+}][AsF_6^-]$ is already observed around 222 K in the tungsten analogue and the second weak transition detected at 61 K in the molybdenum salt transforms into a sharp line width increase at 46 K in the tungsten salt. Low-temperature crystallographic studies would be necessary to ascertain the nature of this second transition, which was much smoother in $[Cp_2Mo(dmit)^{\bullet+}][AsF_6^-]$ where it did not induce any structural changes.

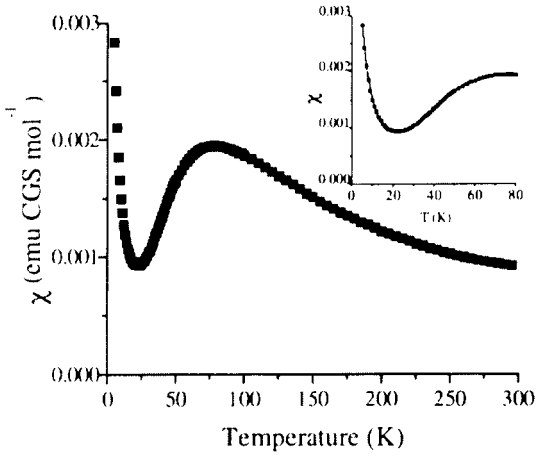

Figure 12. Temperature dependence of the magnetic susceptibility in $[Cp_2W(dsit)^{\bullet+}][AsF_6^-]$. The solid line in the insert is a fit to the spin-ladder model (see text) in the low-temperature range ($R = 0.995$)

Scheme 2

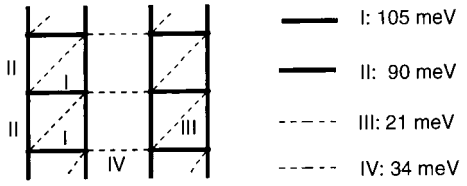

Turning now to the $[Cp_2W(dsit)^{\bullet+}]$ salt, which exhibits a ladder structure, the temperature dependence of the susceptibility (Figure 12) exhibits a Curie−Weiss behavior at the higher temperatures with much stronger antiferromagnetic interactions ($\theta_{Weiss} = -71$ K). Below $T(\chi_{max}) = 78$ K, the activated portion of the susceptibility is characteristic of a spin gap ground state. The ladderlike motif identified in the crystal structure analysis of $[Cp_2W(dsit)^{\bullet+}][AsF_6^-]$ (see above) prompted us to evaluate if such a system could be described as a *spin ladder*, a peculiar magnetic structure known to exhibit such a spin gap. Such systems have been recently the subject of great interest in the solid state physics community,[24] and only a few examples of *molecular* spin ladder structures have been described.[15,25,26] We first calculated the intermolecular interaction energies involved in the four different overlaps identified above (Scheme 2), i.e., the intradimer interaction I (the rungs of the ladder), the interdimer interaction II along *a* (the arms of the ladder), as well as the interactions III and IV, within the ladder and between them. The calculated values reported in Scheme 2 confirm the spin ladder description with indeed much smaller calculated values for interactions III and IV, which can be neglected at this stage. Accordingly, a fit of the activated part of the susceptibility was successfully performed with the formula given by Troyer for spin ladders,[27] taking also into account a low-temperature Curie contribution, and affording a spin gap $\Delta_{gap} = 89$ K. Instead, if we use the numerical simulations developed by Barnes et al. for such spin ladder systems,[28] we deduced antiferromagnetic coupling constants values $|J_\perp| = 165$ K and $|J_{||}| = 90$ K. Even if the ratio $|J_\perp|/|J_{||}|$ value is slightly out of the $0.9 < |J_\perp|/|J_{||}| < 1.1$ domain of validity defined by Barnes et al., it gives a good idea of the coupling values. Indeed, the spin gap value calculated with these coupling constants $|J_\perp|$ and $|J_{||}|$ as $\Delta_{gap} = |J_\perp| - |J_{||}| + J_{||}^2/2|J_\perp| = 99$ K is in excellent accord with the value determined above.

In a Hubbard description,[29] the exchange integral J between radicals can be related to the ratio β^2/U,where β describes the interaction energy between SOMOs and U the energy difference between the (singlet or triplet) ground-state configuration and a charge transfer configuration, that is, $[Cp_2W(dsit)]^0[Cp_2W(dsit)]^{2+}$. The ratio of J values is therefore expected to compare with the ratio of β^2 values. The experimental $|J_\perp|/|J_{||}| = 1.8$ value deduced from the magnetic susceptibility data is indeed close to the calculated $(\beta_I/\beta_{II})^2 = 1.4$ determined by the extended Hückel calculations (Scheme 2). We are therefore faced here with a rare example of a molecular spin ladder system whose formation was made possible thanks the face-to-face dimer association of the Cp_2M(dithiolene) complexes to form the rungs of the ladder. On the other hand, the more symmetric unfolded molecular geometry associated with the orthorhombic structure allows for the setting of a three-dimensional interaction network revealed by the antiferromagnetic ordering below $T_{Néel}$.

Table 3. Electrocrystallization Conditions

	$Cp_2Mo(dsit)$	$Cp_2W(dmit)$	$Cp_2W(dsit)$
m(donor) (mg)	20	17.5	7
m(n-$Bu_4N{\cdot}AsF_6$) (g)	1	0.5	0.1
vol(CH_2Cl_2) (mL)	30	15	15
current (μA)	1 to 5	1.5	1.5
temperature (°C)	15 to −15	−10	20
time (days)	6	15	7

Conclusion

As demonstrated by the DFT calculations, the variety of folding angles and hence the different molecular structures encountered in the open-shell cationic $Cp_2M(dithiolene)^{\bullet+}$ species (M = Mo, W) find their origin in the very low energy cost for distorting those complexes from the C_{2v} geometry up to θ values of 35°. As a consequence, the actual geometry of a complex in a given salt, i.e., its folding angle, and the solid state arrangement of both cation and anion in the crystal are intimately correlated and adapt mutually to each other. Indeed, the energy range involved in this folding process (<1 kcal mol^{-1}) is to be compared with other intermolecular interactions stabilizing solid state structures such as for example "normal" hydrogen bonds (4−15 kcal mol^{-1}) or weaker C−H ···X hydrogen bonds (<4 kcal mol^{-1}).[30] Clearly, here, the molecular flexibility introduces a delicate influence in the stabilization of a given structure. Within these series, a heavy atom effect (W, Se) is however noticeable which stabilizes folded complexes whose SOMO is then not only centered on the dithiolene moiety but also partially delocalized on the metallocene fragment, at the expense of the three-dimensional set of intermolecular interactions observed with the unfolded complexes.

Experimental Section

Synthesis. The complexes were prepared as previously described from Cp_2MoCl_2 or Cp_2WCl_2 (Strem Chemicals) and the $dmit^{2-}$ or $dsit^{2-}$

(24) Dagotto, E.; Rice, T. M. *Science* **1996**, *271*, 618.
(25) (a) Imai, H.; Inabe, T.; Otsuka, T.; Okuno, T.; Awaga, K. *Phys. Rev. B* **1996**, *54*, R6838. (b) Komatsu, T.; Kojima, N.; Saito, G. *Solid State Commun.* **1997**, *103*, 519.
(26) (a) Rovira, C.; Venciana, J.; Ribera, E.; Tarres, J.; Canadell, E.; Rousseau, R.; Mas, M.; Molins, E.; Almeida, M.; Henriques, R. T.; Morgado, J.; Schoeffel, J.-P.; Pouget, J.-P. *Angew. Chem. Int. Ed. Engl.* **1997**, *109*, 22417. (b) Ribera, E.; Rovira, C.; Venciana, J.; Tarres, J.; Canadell, E.; Rousseau, R.; Molins, E.; Mas, M.; Schoeffel, J.-P.; Pouget, J.-P.; Morgado, J.; Henriques, R. T.; Almeida, M. *Chem. Eur. J.* **1999**, *5*, 2025.
(27) Troyer, M.; Tsunetsugu, H.; Würtz, D. *Phys. Rev. B* **1994**, *50*, 13515.
(28) Barnes, T.; Riera, J. *Phys. Rev. B* **1994**, *50*, 6817.
(29) Whangbo, M.-H. *Acc. Chem. Res.* **1983**, *16*, 95.
(30) Desiraju, G. R.; Steiner, T. In *The Weak Hydrogen Bond*; Oxford University Press: New York, 1999.

Table 4. Crystallographic Data

	$Cp_2Mo(dmit)$	$Cp_2W(dsit)$	$[Cp_2W(dmit)][AsF_6]$	$[Cp_2Mo(dsit)][AsF_6]$	$[Cp_2W(dsit)][AsF_6]$
formula	$C_{13}H_{10}MoS_5$	$C_{13}H_{10}S_3Se_2W$	$C_{13}H_{10}AsF_6S_5W$	$C_{13}H_{10}AsF_6MoS_3Se_2$	$C_{13}H_{10}AsF_6S_3Se_2W$
MW	422.45	604.16	699.28	705.17	793.08
crystal system	monoclinic	monoclinic	orthorhombic	orthorhombic	monoclinic
space group	*C*2/*c*	*C*2/*c*	*Cmcm*	*Cmcm*	*P*21/*c*
a (Å)	28.959(6)	29.2720(13)	9.0295(15)	9.071(2)	6.8442(7)
b (Å)	6.627(3)	6.7860(5)	20.568(2)	20.868(4)	15.9923(13)
c (Å)	20.916(4)	20.9123(13)	10.2641(12)	10.243(2)	17.6594(16)
β (deg)	132.77(3)	132.865(9)			90.934(11)
V (Å^3)	2946.7(15)	3044.7(3)	1906.2(4)	1938.9(7)	1932.6(3)
Z	8	8	4	4	4
d_{calc}, mg m^{-3}	1.905	2.636	2.437	2.416	2.726
μ, mm^{-1}	1.579	12.762	8.382	6.499	11.818
F(000)	1680	2224	1316	1332	1460
crystal size	0.24 × 0.12 × 0.03	0.154 × 0.046 × 0.03	0.347 × 0.116 × 0.038	0.22 × 0.08 × 0.014	0.462 × 0.077 × 0.077
θ range	1.92−25.98	2.66−27.81	1.98−25.95	1.95−25.97	1.72−23.98
index range	±8, ±18, 0−19	±38, ±8, ±27	±11, ±25, ±12	±11, 0−25, 0−12	±7, ±18, ±20
refl coll	5601	13678	9180	2522	12078
refl ind	2892	3570	1040	1070	3009
R(int)	0.1589	0.1003	0.0542	0.102	0.0513
abs corr	multiscan	numerical	numerical	psi-scan	numerical
T_{max}, T_{min}	0.959, 0.650	0.4283, 0.142	0.727, 0.319	0.957, 0.656	0.4435, 0.0943
data/rest/par.	2892/0/172	3570/0/172	1040/0/113	1070/0/89	3009/0/235
GOF	0.972	0.861	0.974	1.018	0.873
$R(F)$, $Rw(F^2)$	0.051, 0.139	0.036, 0.075	0.0197, 0.0346	0.033, 0.072	0.0245, 0.0437
res dens	0.855, −1.168	1.68, −1.25	0.48, −0.45	0.60, −0.98	0.56, −0.71

dianions in refluxing THF.[9,15] Electrocrystallization experiments were performed in a two-compartment cell with Pt electrodes (diameter = 1 mm, length = 2 cm) and *n*-$Bu_4N^+AsF_6^-$ as electrolyte in a galvanostatic mode. Details are given in Table 3. Dark, shiny crystals were harvested on the electrode after the indicated time and washed with a small amount of pure CH_2Cl_2. They are stable in air.

X-ray Crystallography. Details about data collection and solution refinement are given in Table 4. Data were collected on a Stoe-IPDS imaging plate system at room temperature except $[Cp_2Mo(dsit)]AsF_6$, which was collected on a Enraf-Nonius Mach3 diffractometer, both operating with a Mo Kα X-ray tube with a graphite monochromator. The structures were solved (SHELXS) by direct methods and refined (SHELXL-93) by full-matrix least-squares methods. Absorption corrections were made for every structure as indicated in Table 4. Hydrogen atoms were introduced at calculated positions (riding model), included in structure factor calculations and not refined. In the orthorhombic structures of $[Cp_2Mo(dsit)]AsF_6$ and $[Cp_2W(dmit)]AsF_6$, the AsF_6^- anion is disordered on two positions and was refined with a fixed 50:50 occupation parameter.

Theoretical Calculations. DFT calculations were performed with Gaussian94[31] using the BPW91 functional with Becke gradient correction for exchange[32] and Perdew−Wang corrections for correlation.[33] A double-ζ basis with electron core pseudopotentials (ECP)(LANL2DZ)[34] was used. Initial geometries were in most cases derived from the X-ray crystallographic studies with the highest possible molecular symmetry, i.e., in the C_s geometry with a symmetry plane containing the metal, the long axis of the dithiolene with the C=S fragment in this plane, and one carbon atom of each cyclopentadienyl ring, therefore imposing a precise Cp orientation. Caccelli et al. have recently shown that the relative orientation of the Cp rings did not significantly affect the total energy of the system.[35]

Magnetic Measurements. Magnetic susceptibility measurements were performed on a Quantum Design MPMS5 SQUID magnetometer operating in the range 5−300 K with polycrystalline samples of $[Cp_2W(dmit)^{\bullet+}][AsF_6^-]$ (5.6 mg) at various fields and $[Cp_2W(dsit)^{\bullet+}][AsF_6^-]$ (22.6 mg) in a 1 T field. Data were corrected for Pascal diamagnetism and sample holder contribution. ESR spectra were collected on oriented single crystals on a Brüker ESP300E equipped with an ESR90 cryostat (4.2−300 K) from Oxford Instruments.

Supporting Information Available: Crystallographic data for the five X-ray crystal structures, in CIF format. This material is available free of charge via the Internet at http://pubs.acs.org.

IC000550Y

(31) Frisch, M. J.; Trucks, G. W.; Schlegel, H. B.; Gill, P. M. W.; Johnson, B. G.; Robb, M. A.; Cheeseman, J. R.; Keith, T.; Petersson, G. A.; Montgomery, J. A.; Raghavachari, K.; Al-Laham, M. A.; Zakrzewski, V. G.; Ortiz, J. V.; Foresman, J. B.; Cioslowski, J.; Stefanov, B. B.; Nanayakkara, A.; Challacombe, M.; Peng, C. Y.; Ayala, P. Y.; Chen, W.; Wong, M. W.; Andres, J. L.; Replogle, E. S.; Gomperts, R.; Martin, R. L.; Fox, D. J.; Binkley, J. S.; Defrees, D. J.; Baker, J.; Stewart, J. P.; Head-Gordon, M.; Gonzalez, C.; Pople, J. A. *Gaussian94*, Revision E.2; Gaussian Inc.: Pittsburgh, PA, 1995.

(32) (a) Becke, A. D. *Phys. Rev.* **1986**, *B33*, 8822. (b) Becke, A. D. *ACS Symp. Ser*. **1989**, *394*, 165. (c) Becke, A. D. *Int. J. Quantum Chem*. **1989**, Symp. No. 23, 599.

(33) Perdew, J. P.; Wang, Y. *Phys. Rev.* **1992**, *B45*, 13244.

(34) (a) Dunning, T. H. Jr.; Hay, P. J. In *Modern Theoretical Chemistry*; Schaefer, H. F., III, Ed.; Plenum Press: New York, 1976; Vol. 1. (b) Hay, P. J.; Wadt, W. R. *J. Chem. Phys.* **1985**, *82*, 270. (c) Hay, P. J.; Wadt, W. R. *J. Chem. Phys.* **1985**, *82*, 284. (d) Hay, P. J.; Wadt, W. R. *J. Chem. Phys.* **1985**, *82*, 299.

(35) (a) Caceli, I.; Keogh, D. W.; Poli, R.; Rizzo, A. *New J. Chem*. **1997**, *21*, 133. (b) Cacelli, I.; Keogh, D. W.; Poli, R.; Rizzo, A. *J. Phys. Chem*. **1985**, *82*, 299.